Optical-resonance-enhanced nonlinearities in a MoS_2-coated single-mode fiber

HAOJIE ZHANG[1,*], NOEL HEALY[2], ANTOINE F. J. RUNGE[1], CHUNG CHE HUANG[1], DANIEL W. HEWAK[1], AND ANNA C. PEACOCK[1]

[1] Optoelectronics Research Centre, University of Southampton, Highfield, Southampton SO17 1BJ, UK
[2] Emerging Technology and Materials Group, School of Electrical and Electronic Engineering, Newcastle University, Newcastle upon Tyne NE1 7RU, UK
[*] Corresponding author: hz15e13@soton.ac.uk

Compiled March 29, 2018

Few-layer molybdenum disulfide (MoS_2) has an electronic band structure that is dependent on the number of layers and is, therefore, a very promising material for an array of optoelectronic, photonic and lasing applications. In this work, we make use of a side-polished optical fiber platform to gain access to the nonlinear optical properties of the MoS_2 material. We show that the nonlinear response can be significantly enhanced via resonant coupling to the thin film material, allowing for the observation of optical modulation and spectral broadening in the telecoms band. This route to access the nonlinear properties of 2D materials promises to yield new insights into their photonic properties.

OCIS codes: *(060.2310) Fiber optics; (190.4390) Non-linear optics, integrated optics; (310.6860) Thin films, optical properties.*

http://dx.doi.org/10.1364/ao.XX.XXXXXX

Owing to their wide range of exceptional properties, two-dimensional (2D) materials including graphene and transition-metal dichalcogenides (TMDCs) have emerged as exciting media for the development of highly functional optoelectronic devices. The most prevalent material in the 2D catalogue is graphene, which has been extensively studied. However, its near zero bandgap energy means that it can be considered a semi-metal, which precludes it from use in a number of important applications such as switching devices like transistors. TMDCs, conversely, are often semiconductors, and their optoelectronic properties can be tuned quite dramatically by controlling the material thickness. For example, in some materials, like MoS_2, it is possible to tune the electronic bandgap from direct to indirect as more layers are added [1].

The layer-dependent bandgap structure puts MoS_2 into an important position for fabricating a variety of optoelectronic devices including gigahertz transistors [2], high sensitivity sensors [3] and integrated circuits [4]. Furthermore, the layer thickness can also be used to control the size of the material's nonlinear coefficients, which is significant for applications involving high power signals. For example, R. Wang *et al.*, have demonstrated third-harmonic generation in ultra-thin films of MoS_2 [5], while several other research groups have compared second and third harmonic generation of monolayer and few-layer MoS_2 using multiphoton microscopy [6–8]. The material's propensity for saturable absorption has also been the subject of many recent articles [9–12].

Here, we focus our investigations on few-layer MoS_2 materials for use in nonlinear optical applications in the telecoms regime. The device is based on a modified side-polished fiber (SPF) design together with a MoS_2/polymer heterostructure that enhances the light-MoS_2 interaction in this wavelength region. Our results show that the interaction of light with the MoS_2 is highly wavelength-dependent, which we attribute to resonant coupling between the MoS_2 and the fundamental mode of the optical fiber. By exploiting the strong nonlinear interaction at the peak of the coupling, all-optical modulation and self-phase modulation are observed with significantly improved efficiencies [9–12]. Thus this work paves the way to the development of practical 2D material-based nonlinear photonic devices for telecoms applications.

A schematic representation of the MoS_2-coated SPF device is shown in Fig. 1(a). A polishing process was developed to produce adiabatic transitions from the fiber's full circular geometry to the uniform D shaped region, which forms the interaction window of ~ 1 cm. To suppress the transmission loss, a cladding buffer of 1 μm was retained across the polishing region. Polishing to this depth permitted access to 30 dB of the light propagating in the SPF and this was confirmed by monitoring the change in transmission when a high index liquid was dropped onto the polished surface. The polishing process was optimized to ensure that the polished surface was parallel to the fiber core along its entire length, which is critical for achieving efficient resonant coupling. Transmission of the fabricated SPF was found to be polarization-independent.

The MoS_2 films were grown by chemical vapor deposition (CVD) onto a 280 nm SiO_2/Si substrate. The process starts through a reaction between the $MoCl_5$ precursor and the H_2S reactive gas at ambient temperature to deposit an amorphous film, followed by an annealing process to create crystalline layers of

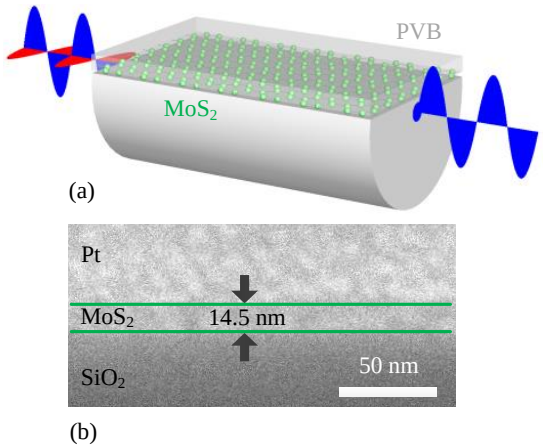

Fig. 1. (a) Schematic model of the PVB-coated MoS_2 device based on a side polished optical fiber. (b) FIB-SEM image of the MoS_2 layer to verify its thickness.

MoS_2 [13]. As the material was crystallized from an amorphous phase, the stacking could be considered as random over a 1 cm length, but AA or AB stacking in the sub-micrometer range. The sample was milled using a focused ion beam (FIB) and imaged using a scanning electron microscope (SEM) to determine the thickness of the MoS_2 film. The sample was coated with platinum prior to the milling process. Fig. 1(b) depicts a SEM image of the cross-section in the milling area. Considering the thickness of a single MoS_2 layer ($\sim 0.6 - 0.7$ nm) [14], the estimated number of layers in our sample is ~ 21. Cross-sectional measurements conducted on several samples prepared via this route indicate that the thickness variation of these MoS_2 layers is on the order of a few nanometers. It is worth noting that the absorption spectrum measured in [13], for a film of similar thickness ($\sim$15 nm), reveals two direct-gap transitions, confirming that the sample's band structure is still in the few-layer regime. Subsequently, a layer of polyvinyl butyral (PVB) was spin-coated to a thickness of 1 μm over the MoS_2 thin film to support the material and improve its durability. The PVB-coated MoS_2 was then separated from the SiO_2/Si substrate using an ultrasonic bubbling method [15], followed by transferring the PVB/MoS_2 film onto the surface of the SPF window to form the device. Significantly, the high index PVB plays a vital role in improving the efficiency of our device as it acts to draw the propagating mode into the 2D-material [16].

The linear transmission properties of the MoS_2-coated fiber device were characterized using a range of laser sources so that the transmitted light could be measured across a broad spectral region. Firstly, a polarized CW source was used to probe the polarization-dependent transmission and it was found that one mode interacted more strongly with the MoS_2 layer. This mode was determined to be the TE mode and the stronger absorption of TE light is due to the positive value of the imaginary part of the dynamic conductivity of MoS_2, in agreement with previous reports [17,18]. As a control experiment, a PVB-only-coated SPF was also tested and no polarization-dependent transmission was observed. Subsequently, the polarisation was fixed so that the TE mode interacted with the over-layer materials and a wavelength tunable source was used to generate the transmission spectrum shown in Fig. 2(a). The strong wavelength dependent spectrum observed, with a 30 dB extinction ratio between $1410 - 1570$ nm,

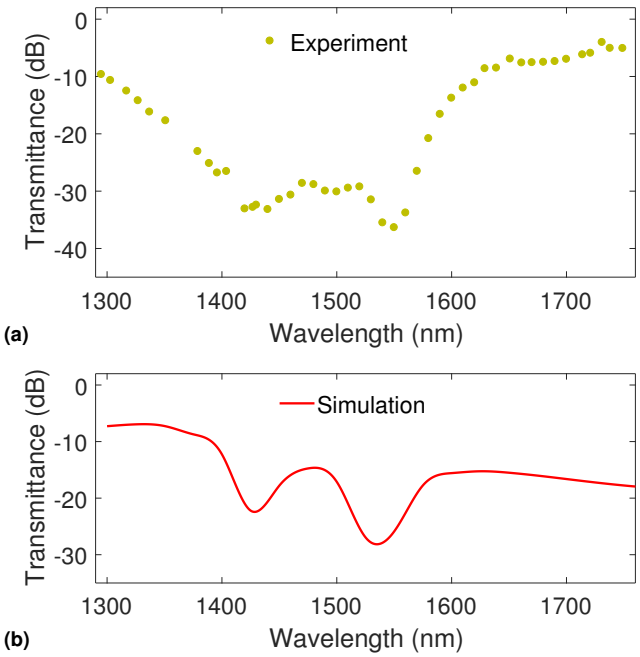

Fig. 2. (a) Experimental absorption spectrum of the MoS_2-coated fiber device ($\sim \pm$ 5% uncertainty for each measurement). (b) Simulated absorption spectrum.

provides evidence that there is resonant coupling between the fundamental mode of the optical fiber and the 2D material. This is in contrast with our previous measurements in graphene-based devices which exhibited a flat absorption behavior [16].

To further investigate the resonant coupling, a numerical study was undertaken using finite-element simulations as described in [19]. In order to match the double dip structure of the experimental curve, we considered a slight variation in the film thickness across the 1 cm long MoS_2 sample. Fig. 2(b) shows the simulated spectrum with a coupling dip at 1420 nm, corresponding to a layer thickness of 10 nm, and at 1540 nm, corresponding to a thickness of 13 nm, both in close agreement with measured film in Fig. 1(b). The qualitative agreement with the experimental results indicates that there is indeed resonant coupling between the fiber mode and the MoS_2 layer, which could be optimized for access to different wavelength regions. Since the resonant peak is closely related to the thickness of the MoS_2 layer, the nonlinear enhancement could also be broadened to cover the entire telecoms band by using a MoS_2 film with a varying thickness. We note that additional simulations have shown that the resonant coupling is not related to the thickness of the PVB layer.

To demonstrate the enhanced nonlinear characteristics of the device when operated on resonance, transmission measurements were conducted using a low-noise, high power femtosecond fiber laser (Onefive Origami 15) with a central wavelength of $\sim$ 1542 nm, a pulse duration of 750 fs FWHM, and a repetition rate of 40 MHz. The laser's output power was controlled using a variable optical attenuator and its polarization state was varied using a polarization controller. Fig. 3 shows the transmittance of the TE and TM modes as a function of increasing average power and there is a clear onset of nonlinear saturable absorption of the TE mode. Specifically, up to $P_{ave} \sim 3$ mW (corresponding to a peak power of $P_p \sim 94$ W) the transmittance of the TE mode

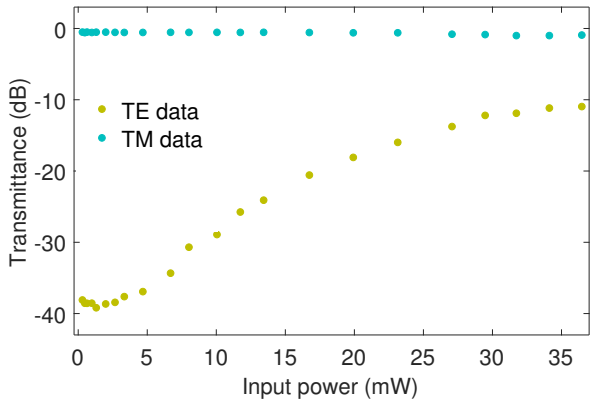

Fig. 3. Nonlinear saturable absorption measurements ($\sim \pm 5\%$ uncertainty for each measurement). Transmittance of MoS_2-coated fiber device as a function of average input power.

stays around -38 dB. However, for higher input powers the absorption becomes nonlinear and the transmitted light starts to increase rapidly, eventually reaching a saturable transmittance of -11 dB for $P_{ave} \sim 36$ mW ($P_p \sim 1127$ W), meaning a 27 dB change of the TE mode transmittance. In contrast, the transmission of the TM mode remains linear and changes less than 0.5 dB as there is minimal interaction between the TM mode and the MoS_2 sheet.

The nonlinear spectral properties of the device were then examined using a similar experimental set-up, but with the output connected to an optical spectrum analyzer (OSA). Fig. 4 shows the output spectra at different input powers of the TE mode, clearly showing the onset of self-phase modulation-based spectral broadening. The output spectrum changes from 12 nm to 59 nm at the -20 dB intensity level when the input peak power increases from 40 W to 642 W. This level of broadening (2.44 nm/mW) is remarkable considering the incredibly small volume of MoS_2 that the light is interacting with. In order to quantify the role of the highly nonlinear MoS_2 film, we determined the size of the effective nonlinear coefficient (γ) in this section of the fiber by fitting the spectral broadening with the nonlinear Schrodinger equation [20]. From this modeling, we estimate γ in the device to be around 1000 times larger than standard SMF, and about 30 times larger than highly nonlinear

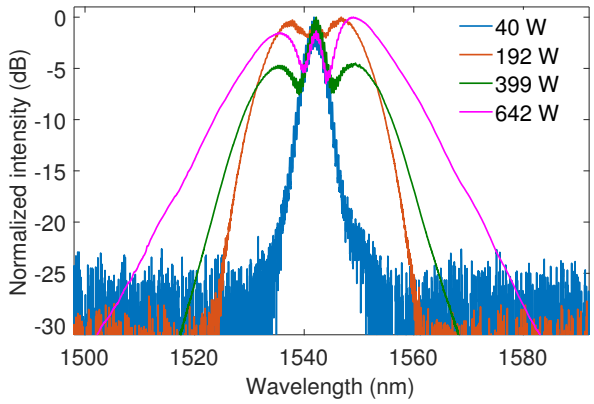

Fig. 4. Output spectral evolution at different input peak powers to illustrate spectral broadening.

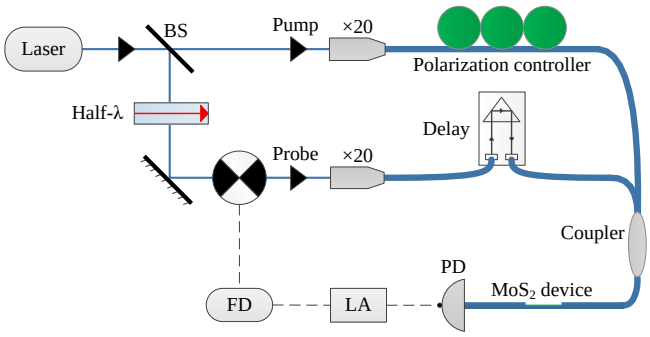

Fig. 5. Schematic illustration of the experimental set-up used for high intensity optical characterization. BS: beam splitter; FD: frequency driver; LA: lock-in amplifier; PD: photodiode.

fibers such as small core microstructured designs [21,22]. We note that two control experiments were undertaken for comparison with this system. In the first, the TM mode was launched in to the MoS_2 device, and in the second, TE light was launched in to a PVB only coated fiber. In both cases, no spectral broadening was observed. Thus, this effect can be entirely attributed to the TE mode's interaction with the MoS_2 film. These experiments were then repeated at the additional wavelengths of 1300 nm, 1350 nm, 1450 nm and 1500 nm. As expected, spectral broadening was observed when on resonance at the longer wavelengths, while no broadening was observed at 1300 nm and 1350 nm. We believe that the strong interaction measured in this device within the telecoms band provides clear evidence of the resonance-enhanced light-matter interaction.

A further experiment was undertaken to test the suitability of the MoS_2 material for the development of high-speed all-optical modulators, similar to what has been achieved in graphene [19]. In this experiment a time-resolved optical pump-probe technique was used to determine the fast temporal resolution of all-optical modulation in the PVB-coated-MoS_2 fiber device. The experimental set-up is shown in Fig. 5. The output beam of the Origami fiber laser was split into a high power pump ($P_{ave} \sim 35.3$ mW, $P_p \sim 1105$ W) and a weak probe component ($P_{ave} \sim 711\,\mu$W, $P_p \sim 22$ W). The probe was modulated at 100 Hz

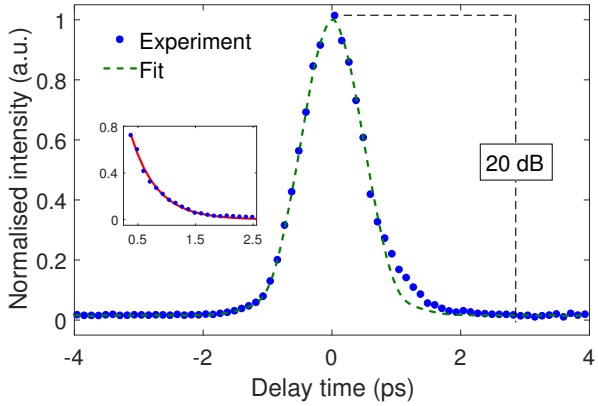

Fig. 6. Normalised intensity of the probe light as a function of the pump-probe time delay. The green dashed line is an overlay of the pump pulse to highlight the slow falling edge. Inset: exponential fit of the falling edge.

using an optical chopper connected to a lock-in amplifier to discriminate between the two signals. Polarization controllers were used to ensure that both the pump and probe were aligned so that they efficiently coupled into the MoS_2 layer. A 10 ps adjustable delay line was inserted into the path of the probe to control the temporal overlap of the two pulses. The pump and probe pulses were then recombined using a fused tapered coupler before being connected to the input arm of the device. Fig. 6 shows that the power of the transmitted probe signal can be modulated over a time-scale of 2 ps as the pump-probe overlap is tuned. A modulation depth of 20 dB was achieved, calculated as the ratio between the maximum and minimum transmittance [23]. Compared to the graphene-based counterpart device [19], the higher modulation depth measured in the MoS_2 fiber device (around 11 dB) is attributed to the resonance-enhanced light-matter interaction within the telecoms band. The green line in Fig. 6 is an overlay of the pump pulse, included to highlight the slower falling edge of the modulated signal, which is due to the carrier recovery in the MoS_2 sheet. The carrier relaxation process occurs on a time-scale estimated to be $\tau \sim 0.5$ ps by fitting the decaying response with an exponential fit, as shown in the inset of Fig. 6.

In conclusion, a MoS_2-based all-optical modulator with a high extinction ratio of 20 dB and a low loss of 0.5 dB has been designed and experimentally demonstrated in the telecoms band. When compared to previous devices, our method results in a resonance-enhanced interaction with the MoS_2 sheet to produce a significant increase in modulation depth. We believe that the strong wavelength-dependent interaction measured in this device provides clear evidence of the resonance-enhanced light-matter interaction. Spectral broadening was also observed in the ~ 14 nm MoS_2 sheet, providing additional evidence of the strong interaction with the fiber's propagating mode. With further optimization of the device design and number of material layers, we predict that these structures will find use in wide-ranging nonlinear optical applications, including those based on the second order processes (e.g., second harmonic generation). Thus, not only does this device design provide an excellent test bed for studying the nonlinear properties of 2D materials, but it also lays a clear pathway for such materials to be used in real world applications.

Funding. The authors acknowledge EPSRC for financial support through EP/P000940/1 and the Future Photonics Hub (EP/H02607X/1).

Acknowledgment. Haojie Zhang thanks the China Scholarship Council for financial support. The data for this Letter are accessible through the University of Southampton Institutional Research Repository.

REFERENCES

1. K. F. Mak, C. Lee, J. Hone, J. Shan, and T. F. Heinz, Phys. Rev. Lett. **105**, 136805 (2010).
2. D. Krasnozhon, D. Lembke, C. Nyffeler, Y. Leblebici, and A. Kis, Nano Lett. **14**, 5905 (2014).
3. F. K. Perkins, A. L. Friedman, E. Cobas, P. Campbell, G. Jernigan, and B. T. Jonker, Nano Lett. **13**, 668 (2013).
4. Y. Zhang, J. Ye, Y. Matsuhashi, and Y. Iwasa, Nano Lett. **12**, 1136 (2012).
5. R. Wang, H.-C. Chien, J. Kumar, N. Kumar, H.-Y. Chiu, and H. Zhao, Appl. Mater. Interfaces **6**, 314 (2013).
6. A. Säynätjoki, L. Karvonen, H. Rostami, A. Autere, S. Mehravar, A. Lombardo, R. A. Norwood, T. Hasan, N. Peyghambarian, H. Lipsanen *et al.*, Nat. Commun. **8**, 893 (2017).
7. L. Karvonen, A. Säynätjoki, M. J. Huttunen, A. Autere, B. Amirsolaimani, S. Li, R. A. Norwood, N. Peyghambarian, H. Lipsanen, G. Eda *et al.*, Nat. commun. **8**, 15714 (2017).
8. R. Woodward, R. Murray, C. Phelan, R. de Oliveira, T. Runcorn, E. Kelleher, S. Li, E. de Oliveira, G. Fechine, G. Eda *et al.*, 2D Mater. **4**, 011006 (2016).
9. K. Wang, J. Wang, J. Fan, M. Lotya, A. O Neill, D. Fox, Y. Feng, X. Zhang, B. Jiang, Q. Zhao *et al.*, ACS Nano **7**, 9260 (2013).
10. S. Wang, H. Yu, H. Zhang, A. Wang, M. Zhao, Y. Chen, L. Mei, and J. Wang, Adv. Mater. **26**, 3538 (2014).
11. J. Du, Q. Wang, G. Jiang, C. Xu, C. Zhao, Y. Xiang, Y. Chen, S. Wen, and H. Zhang, Sci. Rep. **4**, 6346 (2014).
12. R. Woodward, E. Kelleher, R. Howe, G. Hu, F. Torrisi, T. Hasan, S. Popov, and J. Taylor, Opt. Express **22**, 31113 (2014).
13. C.-C. Huang, F. Al-Saab, Y. Wang, J.-Y. Ou, J. C. Walker, S. Wang, B. Gholipour, R. E. Simpson, and D. W. Hewak, Nanosc. **6**, 12792 (2014).
14. C. Lee, H. Yan, L. E. Brus, T. F. Heinz, J. Hone, and S. Ryu, ACS Nano **4**, 2695 (2010).
15. D. Ma, J. Shi, Q. Ji, K. Chen, J. Yin, Y. Lin, Y. Zhang, M. Liu, Q. Feng, X. Song *et al.*, Nano Res. **8**, 3662 (2015).
16. H. Zhang, N. Healy, L. Shen, C. C. Huang, N. Aspiotis, D. W. Hewak, and A. C. Peacock, J. Lightwave Technol. **34**, 3563 (2016).
17. Y. Tan, R. He, C. Cheng, D. Wang, Y. Chen, and F. Chen, Sci. Rep. **4**, 7523 (2014).
18. Z. Li and J. Carbotte, Phys. Rev. B **86**, 205425 (2012).
19. H. Zhang, N. Healy, L. Shen, C. C. Huang, D. W. Hewak, and A. C. Peacock, Sci. Rep. **6**, 23512 (2016).
20. G. P. Agrawal, *Nonlinear Fiber Optics* (Academic Press, 2012).
21. Y. Yamamoto, Y. Tamura, and T. Hasegawa, SEI Tech. Rev. **83**, 15 (2016).
22. K. Saitoh and M. Koshiba, Opt. Express **12**, 2027 (2004).
23. Z. Sun, A. Martinez, and F. Wang, Nat. Photon. **10**, 227 (2016).